Molecular rotors in haemoglobin and bovin serum albumin proteins

Alice Briole, Bérengère Abou

Molecular rotors in haemoglobin and bovine serum albumin proteins

Alice Briole and Bérengère Abou

Matière et Systèmes Complexes, UMR7057 CNRS - Université Paris Cité, 75205 Paris, France

ABSTRACT

Molecular rotors are fluorescent viscosity probes and their response in simple fluids is known to be a Förster-Hoffman power law, allowing the viscosity of the medium to be quantified by its fluorescence intensity. They are attractive probes in biological media, usually consisting of proteins, but how does a molecular rotor behave in a protein solution ? The response of the DASPI molecular rotor is compared in two globular protein solutions of similar size, haemoglobin (Hb) and bovine serum albumin, one absorbent, the other not. In absorbent Hb, a model validated by experiments in triangular geometry allows to correct the absorbing effect and to compare the rotor response in both proteins. With concomitant microrheology measurements, we investigate the relation between the DASPI fluorescence intensity and solution viscosity. In protein solutions, we show that viscosity is no longer the parameter determining the rotor response in contrast to simple fluids. Varying the viscosity by concentration or temperature is not equivalent, and the Förster-Hoffmann power laws do not apply when the solution concentration varies. We show that the concentration regime of the protein solution, semi-dilute or concentrated, determines the sensitivity of the rotor to its environment.

1 Introduction

Molecular rotors are fluorescent molecules, now well-established as viscosity probes. After photoexcitation, their relaxation occurs either by fluorescent radiation or by non radiative intramolecular rotation. In a highly constrained environment, the predominant decay pathway is radiative, which leads to a large increase in the fluorescence quantum yield. In simple fluids, it was demonstrated that their quantum yield ϕ increases with the fluid viscosity η according to the Förster-Hoffmann equation[1–8]:

$$\log \phi = C + x \log \eta \tag{1}$$

where C and x are solvent- and dye- dependent constants. The exponent is a constant of $x = 2/3$ in the derivation of the Förster and Hoffmann model[1], but it can be variable according to the free-volume theory by Loutfy et al.[4]. This relationship (1) has been extensively investigated and validated in a wide range of viscosities, in both polar and non polar fluids[5,6,8,9]. Molecular rotors have proven their value in a variety of applications such as the real-time monitoring of aggregation and polymerization processes (PMMA, chain entanglement of macromolecules)[10,11], investigation of phospholipid bilayers and cell membranes[5,12–14]. Recent studies have focused on the development of new fluorescent probes with specific properties for imaging biological materials: low toxicity, good stability, high sensitivity to small variations in microviscosity or specific localisation in biological media[15–18]. BODIPY fluorophores are particularly interesting in this context as they have good photophysical properties and can easily be functionalized[16]. In addition, numerous studies have focused on the use of molecular rotors in proteins to study the effects of aggregation and protein conformational changes[6,19–24] or to detect proteins in living cells and specific biomolecular interactions[25–27].

Recently, we have demonstrated the utility of the DASPI molecular rotor in the assessment of the intracellular viscosity of red blood cells as a function of temperature[28], paving the way for applications in the diagnosis of red blood cell pathologies. DASPI is well adapted to the characterisation of haemoglobin (Hb), the major component protein of the red blood cell, as its fluorescence excitation and emission spectrum interfere little with the fluorescence spectrum of Hb. Although positioned in the region of absorbance minima, between $550-600$ nm[29], the emission signal by the rotor is still subject to a low absorbance of Hb, which may affect the interpretation of this emission signal in terms of rheological properties. More generally, compared to simple fluids, protein solutions are complex because of the structure of the proteins themselves and the resulting assembly in solution. At the molecular rotor scale, complex interactions with proteins, such as binding[3,22], localisation to a specific area[15,16], are possible and may affect its response. Given the diversity and complexity of proteins, the determination of rotor response will require extensive studies, taking into account the specificity of each rotor-protein pair.

In this perspective, we study the capacity of the molecular rotor DASPI to characterize the viscosity of two protein solutions, bovine serum albumin (BSA) and Hb. The two globular proteins have a similar molecular weight around 65kDa, and at the

absorption and emission wavelengths of DASPI, Hb is optically absorbent whereas BSA is not. We propose a correction model for the absorbance of Hb, based on Beer Lambert's law, which will be used to compare the rotor response in the two proteins. The correction model is detailed and validated in the Appendix, in a geometry of increasing thickness that allows the probing of increasing absorbance levels. The viscosity of the protein solutions, measured by microrheology, is varied either by concentration (section 3.1) or by temperature (section 3.2). Microrheology and rotor fluorescence measurements were carried out concomitantly in the protein solutions. With concentration, the signal emitted by the rotor follows a master curve, which saturates at high viscosity. It does not follow a Förster-Hoffmann law. With temperature, on the other hand, we measure Förster-Hoffmann power laws, with a parameter C that depends on the concentration of the solution. Varying the concentration or temperature is therefore not equivalent in protein solutions, unlike what is measured in simple fluids with C independent on temperature[28,30] and concentration. This highlights that viscosity is not the predominant factor of the rotor response in proteins. The concentration regime of the protein solution, semi-dilute or concentrated, determines the sensitivity of the rotor to its environment and must be considered.

2 Materials and Methods

2.1 Preparation of protein solutions

Human haemoglobin from red blood cells The Hb (molar mass 64 kDa[31]) was extracted from human red blood cells. Blood samples were obtained from healthy donors and provided by the Etablissement Français du Sang (EFS Rhône-Alpes). The red blood cells were washed three times in PBS buffer. After a final centrifugation at $1200 \times g$ for 10 min, all supernatant was removed. The RBC pellet was exposed to 3 freeze-thaw cycles (from -80°C to 37° C) to lyse the RBC membranes. Membrane residues were then extracted by adding of CCl_4 to the lysate ($1/3$ of the volume), followed by strong agitation and ultra-centrifugation at $10000 \times g$ for 15 min. From this stock Hb solution, phosphate-buffered saline (PBS) was used for dilution. The concentration of the stock solution was carried out using 300 000 MWCO Vivaspin 2 Centrifugal Concentrators (Sartorius) by centrifugation at $4500 \times g$ and 37° C for 30mn. The concentration of Hb solutions was varied between 2g/dL and 42g/dL and measured by colorimetry with a MAK 115 Hb Assay Kit (Sigma-Aldrich).

Bovine serum albumin solutions BSA solutions (molar mass 66 kDa) were prepared by diluting lyophilized BSA powder (Sigma-Aldrich) in PBS (phosphate buffered saline, 1X, pH=7.4). The BSA concentration of the solutions, ranging from 1g/dL to 54g/dL, was measured by colorimetry with the Bradford Comassie Blue test (Sigma-Aldrich).

2.2 Measurement geometries: standard and triangular

Microrheology and fluorescence measurements were performed together on the same sample containing the protein solution, Hb or BSA. The solutions were placed in a standard geometry, consisting of a glass slide and a coverslip separated by a 250 µm thick spacer (see Figure 5a in Appendix A). For the Hb solutions, a triangular geometry was also used, which gives access to several levels of absorbance of the solution. In this case, the Hb solution is placed between two coverslips separated by a 250 µm high spacer on one side, creating an increasing thickness from 0 to 250 µm across the chamber (see Figure 5b in Appendix A).

2.3 Particle tracking microrheology

The viscosity of the protein solutions was measured using particle tracking microrheology. This technique consists of investigating the Brownian motion of microscopic probe particles embedded in the fluid to deduce its rheological properties[32]. Typically, microrheology experiments are performed on small volumes of the order of 1µL. This is of interest in biological samples where tiny volumes can be probed, such as recently insect secretion with 10 pL of liquid[33]. Another important aspect in complex fluids is to be able to probe the spatial heterogeneity of the fluid by comparing the response of different probe beads at different locations in the sample[34].

Calibrated Polystyrene beads (0.994 μm in diameter) were dispersed in the solutions to be studied at a low volume fraction of less than 1%. The thermal motion of the tracer beads was recorded for 20 s at 100 Hz with a fast sCMOS camera (OrcaFlash4.0 v2+, Hamamatsu Photonics France) mounted on a Leica DMI 8 (Leica Microsystems GmbH, Germany) inverted bright-field microscope at 100X magnification (oil immersion objective, $NA = 1.3$, depth of field: ~ 200 nm). The sample temperature was controlled with an objective heater using immersion oil in contact with the sample (Bioptechs Inc., USA) to within ± 0.1°C. A custom image analysis software allowed to track the x and y positions of any beads close to the objective focus plane. For reliable analysis, special attention was brought to record only beads far from the surfaces of the glass slides in the standard or triangle geometries.

For each tracer bead i, the time-averaged mean-squared displacement was calculated according to $<\Delta r_i^2(t)> = <(x_i(t+t') - x_i(t'))^2 + (y_i(t+t') - y_i(t'))^2>_{t'}$. For a homogeneous sample, which is the case for our protein solutions at any concentration, the MSD is then averaged over all the beads to determine the ensemble-averaged MSD, $\langle \Delta r^2(t) \rangle$. In case where the MSD

grows linearly with time t, which is the signature of a viscous fluid (without an elastic component), a diffusion coefficient D is determined according to $<\Delta r^2(t)>=4Dt$ (in two dimensions). The viscosity η can then be estimated with the Stokes–Einstein relation, $D = kT/6\pi R\eta$, with R the diameter of the bead and kT the thermal energy[35].

2.4 Fluorescence microscopy

Measurements of the DASPI molecular rotor response in protein solutions were performed by fluorescence microscopy (Leica DMI 8, Leica Microsystems GmbH, Germany) with excitation between $460-500$ nm and detection between $565-625$ nm at $100X$ magnification in the standard geometry and at $63X$ magnification in the triangular geometry. Images were recorded with the fast sCMOS camera (OrcaFlash4.0 v2+, Hamamatsu Photonics France). Intensity measurements of the fluorescence level of the images were performed using ImageJ software (ImageJ, Rasband, W.S., ImageJ, U. S. National Institutes of Health, Bethesda, Maryland, USA, https://imagej.nih.gov/ij/, 1997-2018).

3 Results

3.1 Molecular rotor response with concentration

3.1.1 Absorbance correction and intensity-viscosity master curve in protein solutions

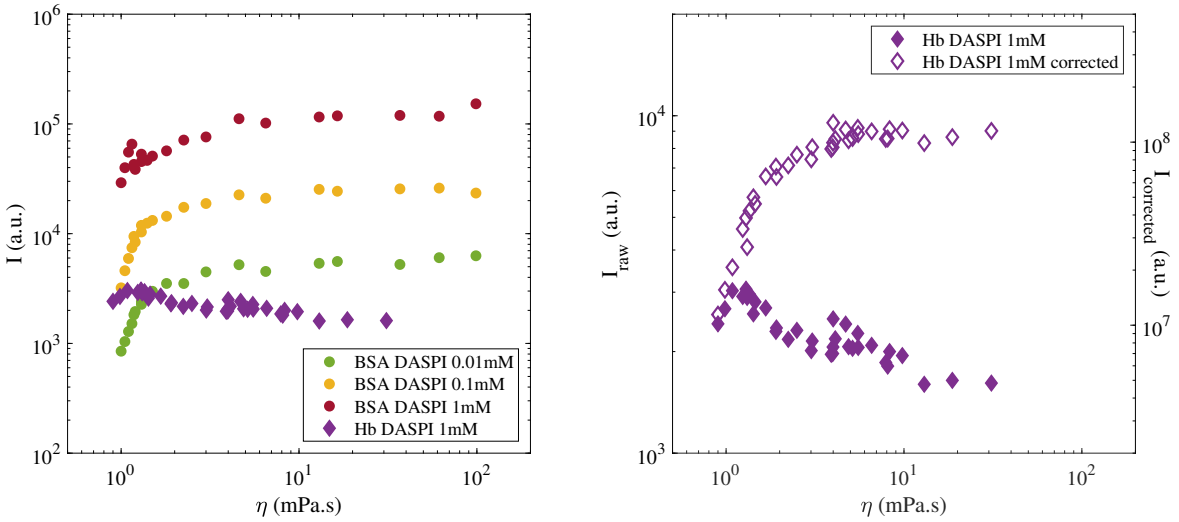

Figure 1. Left: Fluorescence intensity of the DASPI molecular rotor (in arbitrary units, a.u.) as a function of solution viscosity, in BSA and Hb, in the standard geometry at temperature $T = 25°C$. The rotor concentration is adjusted to 0.1, 0.01 and 1 mM in BSA and 1 mM in Hb. In BSA solutions, the rotor response increases with increasing viscosity. In contrast, in Hb solutions, the rotor signal decreases with increasing solution viscosity, due to the increase in solution absorbance with concentration. Right: Intensity - viscosity response of DASPI molecular rotor at 1 mM concentration in Hb solutions: raw data (solid symbols) and absorbance-corrected data (empty symbols). The margins of error are of the order of magnitude of the marker size in both directions: 5% for viscosity measurements and 7% for intensity measurements.

The response of the DASPI molecular rotor was studied in BSA and Hb protein solutions of increasing viscosity as a result of increasing concentration. Figure 1 - (left) shows the fluorescence intensity of the rotor as a function of solution viscosity. In BSA solutions, the intensity emitted by the rotor increases overall with increasing viscosity, whereas it decreases with increasing viscosity in Hb solutions, due to the increase in absorbance of the solution with increasing concentration. In Figure 1 - (right), the intensity emitted by the rotor in Hb solutions has been corrected for the absorbing term (see Appendix A for details), and the corrected and uncorrected signal from the rotor are displayed. With the correction, the signal from the rotor in Hb increases with viscosity as in the case in BSA, and two rotor response regimes – low and high viscosity – are detectable on the intensity-viscosity curves.

As the emitted intensity is a quantity expressed in arbitrary units, the BSA and Hb curves were matched at the same level, to reveal a master curve reflecting the rotor response in our protein solutions (Figure 2). At low viscosity, the emitted intensity increases sharply according to a power-law, $\log I = C + b\log\eta$, with an exponent $b = 3.4$ greater than $2/3$ measured in simple fluids, indicating a high sensitivity of the rotor to the protein environment. At high viscosity, the rotor response reaches a plateau, giving evidence of a lack of sensitivity to viscosity in this second regime. Without doubt, in these protein solutions,

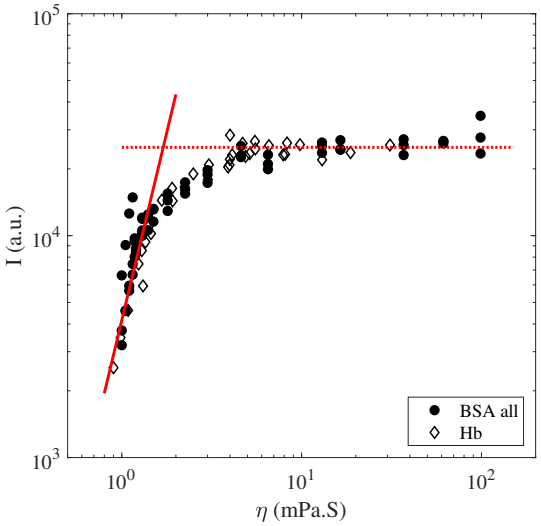

Figure 2. Master curve of the rotor response in BSA and Hb protein solutions of increasing viscosity, at temperature $T = 25°C$. The rotor signal in Hb solutions is corrected for the absorbance of Hb. Two regimes are visible: at low viscosity, the rotor signal increases strongly with viscosity, while at high viscosity, the rotor signal saturates and reaches a plateau. The first regime was fitted by a power-law $\log I = C + b \log \eta$ with $C = 4.1 \cdot 10^3$ and $b = 3.4$ (red solid line) and the second by a constant value $I = 2.5 \cdot 10^4$ in arbitrary units (red dotted line). We do not observe a Förster-Hoffmann power-law over the entire viscosity range as in simple fluids. At low viscosities where a power law behaviour is measured, note that the exponent b is larger than the $2/3$ expected for a Förster-Hoffmann relation.

the rotor does not respond according to a Förster-Hoffmann power-law over the entire viscosity range as observed in simple fluids[8,28].

3.1.2 Response of the molecular rotor in the semi-dilute and concentrated regime

In this section, we compare the response of the two probes – fluorescence intensity for the molecular rotor and viscosity for the Brownian beads – as a function of the concentration of the protein solutions (Figure 3). Each probe interacts with the surrounding medium at its own scale, sub-nanometric for the rotor and micrometric for the Brownian bead.

We first describe the response of the Brownian beads, i.e. the viscosity-concentration curves. The viscosity of both BSA and Hb solutions increases slowly at low concentration and then quite drastically at higher concentration, reminiscent of the characteristic signature of hard-sphere colloids[36–38], widely used in globular proteins to account for this drastic increase[39–45]. Although the comparison between globular proteins (with anisotropic 3D structure, polydispersity, surface charges and anisotropic interactions) and hard spheres is questionable, especially at high concentrations[46,47], this allows the radius of the globular protein to be estimated at low concentration with an Einstein-Batchelor model[48]. This model describes the viscosity of hard-sphere suspensions in the semi-dilute regime (volume fraction less than $\Phi \sim 0.2$) where only the interactions between two particles are taken into account. At higher volume fractions, we enter the concentrated regime where empirical equations of the Mooney[49] or Krieger & Dougherty[50] type are used to describe the drastic viscosity increase. At low concentration below 12g/dL, the radii of the BSA and Hb proteins could be estimated to be 3.3 ± 0.2 nm and 3.6 ± 0.2 nm respectively, in accordance with the literature on the subject[45,51–54]. We verify a posteriori by assimilating the protein to a sphere of the radius found experimentally that this limit concentration, 12g/dL, corresponds to volume fractions, $\Phi \sim 16\%$ in BSA and $\Phi \sim 22\%$ in Hb, consistent with the boundary between the semi-dilute and concentrated regimes in hard spheres.

We now analyse the rotor response with the protein concentration. We observe two power-law regimes with a higher exponent at low concentration (1.1 in BSA and 0.8 in Hb) than at high concentration (0.6 in BSA and Hb). The cross-over between the two regimes is observed for $c_{BSA} = 10.4$g/dL ($\Phi \simeq 14\%$) in BSA and $c_{Hb} = 11$g/dL ($\Phi \simeq 20\%$) in Hb, close to the upper limit of the semi-dilute regime probed in microrheology. This highlights a decrease in rotor sensitivity beyond the semi-dilute regime, which suggests a sensitivity of the rotor to its environment and a screening of its response with crowding.

From the curves in Figure 3, we can see that each probe detects the boundary between the semi-dilute and concentrated regimes. The fact that the Brownian beads and the rotor do not probe the protein solutions at the same scale explains why the semi-dilute regime is not exactly seen at the same concentration by both types of probes.

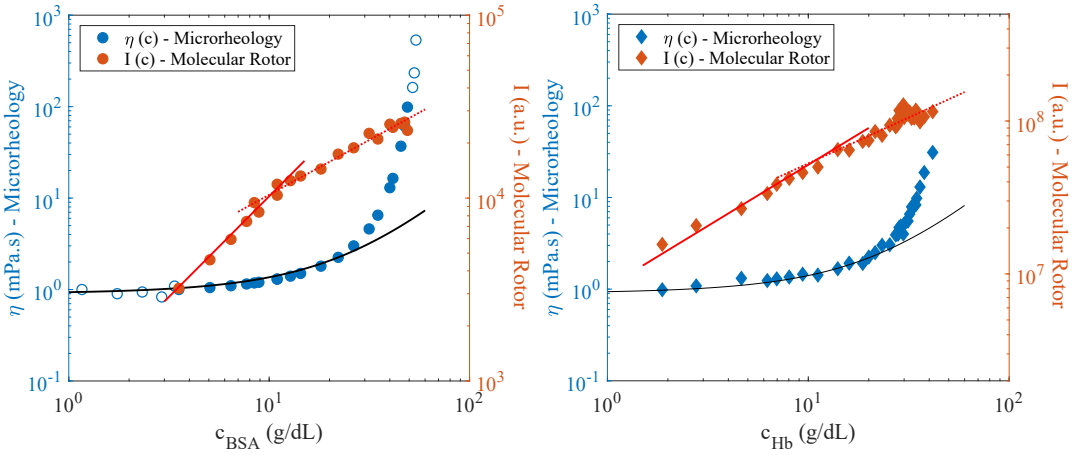

Figure 3. Viscosity measured by microrheology and fluorescence intensity measured by the DASPI rotor, in solutions of BSA (left) and Hb (right) of increasing concentration, at temperature $T = 25°C$. In Hb solutions, the intensity emitted by the rotor was corrected for the absorbance term. Empty markers are used for solutions where only the viscosity has been measured. The DASPI concentration is set at 0.1 mM in BSA and 1mM in Hb. The black solid curve on the viscosity curves correspond to the Einstein-Batchelor model describing the semi-dilute regime of hard sphere suspensions, and allows the radius of each globular protein and the extent of the semi-dilute regime to be estimated. The rotor response shows two power-law regimes, at high (exponent 0.6 in BSA and Hb) and low (exponent 1.1 in BSA and 0.8 in Hb) concentration (red solid and dotted lines). Each probe, Brownian bead and rotor, although probing at different scales, seems to detect the transition from the semi-dilute to concentrated regime.

3.2 Molecular rotor response with temperature

In the previous sections, the viscosity of the protein solutions was varied with concentration. Here we vary the temperature – 18°C, 25°C, 30°C, 37°C and 43°C – at a fixed concentration, which induces a variation in viscosity of up to 30%. Figure 4-(a,b) represents the fluorescence response of DASPI with temperature variations, plotted as a function of the viscosity, in protein solutions of different concentrations. The rotor fluorescence signal increases with viscosity and depends on the concentration of the protein solution. The intensity-viscosity curves are plotted at the same origin (Figure 4-(c,d)) and all data are adjusted to a Förster-Hoffmann power law $I/I_{43°C} = C\,(\eta/\eta_{43°C})^x$. Exponents $x = 0.7 \pm 0.2$ in BSA and $x = 0.9 \pm 0.2$ in Hb are found, they are close to those predicted for simple fluids $x = 0.7$[6,8]. With the determined and fixed x values, the parameter C is found to decrease sharply at high concentration (insets in Figure 4-(c,d)). Therefore, for a given viscosity value in Figure 4-(a,b), there may be different rotor intensities, depending on the concentration of the solution, highlighting that viscosity is not the relevant parameter to describe the rotor response in protein solutions. The concentration of the solution determines the response of the rotor through the parameter C, which again suggests that the response of the rotor depends on the crowding of the environment.

4 Discussion and conclusion

We study the signal emitted by a molecular rotor, DASPI, in two protein solutions, BSA and Hb, and show that its response with viscosity differs when varying concentration or temperature. The two globular proteins are the same size, and one is absorbent while the other is not. We propose a simple model based on Beer Lambert's law, that takes into account the configuration of our set-up and allows to correct for the effect of Hb absorbance. The correction term depends on the Hb concentration c_{Hb} and the chamber height L via a screening length $L_e = 50 - 200\,\mu$m which is a characteristic length of absorbance (see Appendix A). With the correction, the rotor signal in the absorbing Hb and in the non-absorbing BSA can thus be compared.

Let us recall some results obtained in simple fluids with the molecular rotor DASPI. In glycerol and ethylene glycol solutions, we measured its response with viscosity by concentration or temperature variation. With concentration variation, the DASPI fluorescence intensity follows a Förster-Hoffmann power-law over $1.5 - 2$ decades of viscosity, with a parameter C depending on the fluid-rotor couple and the rotor concentration[28]. We measured that C does not depend on the the solution concentration, and that the viscosity is the only parameter that determines the quantum yield of the rotor. This has already been described extensively in previous studies where the Förster-Hoffmann power-law relationship between quantum yield and viscosity was measured over more than three orders of magnitude of the solvent viscosity[8,55]. By temperature variation, we measured that the rotor signal follows the same Förster-Hoffmann power-law as by varying the concentration, corresponding

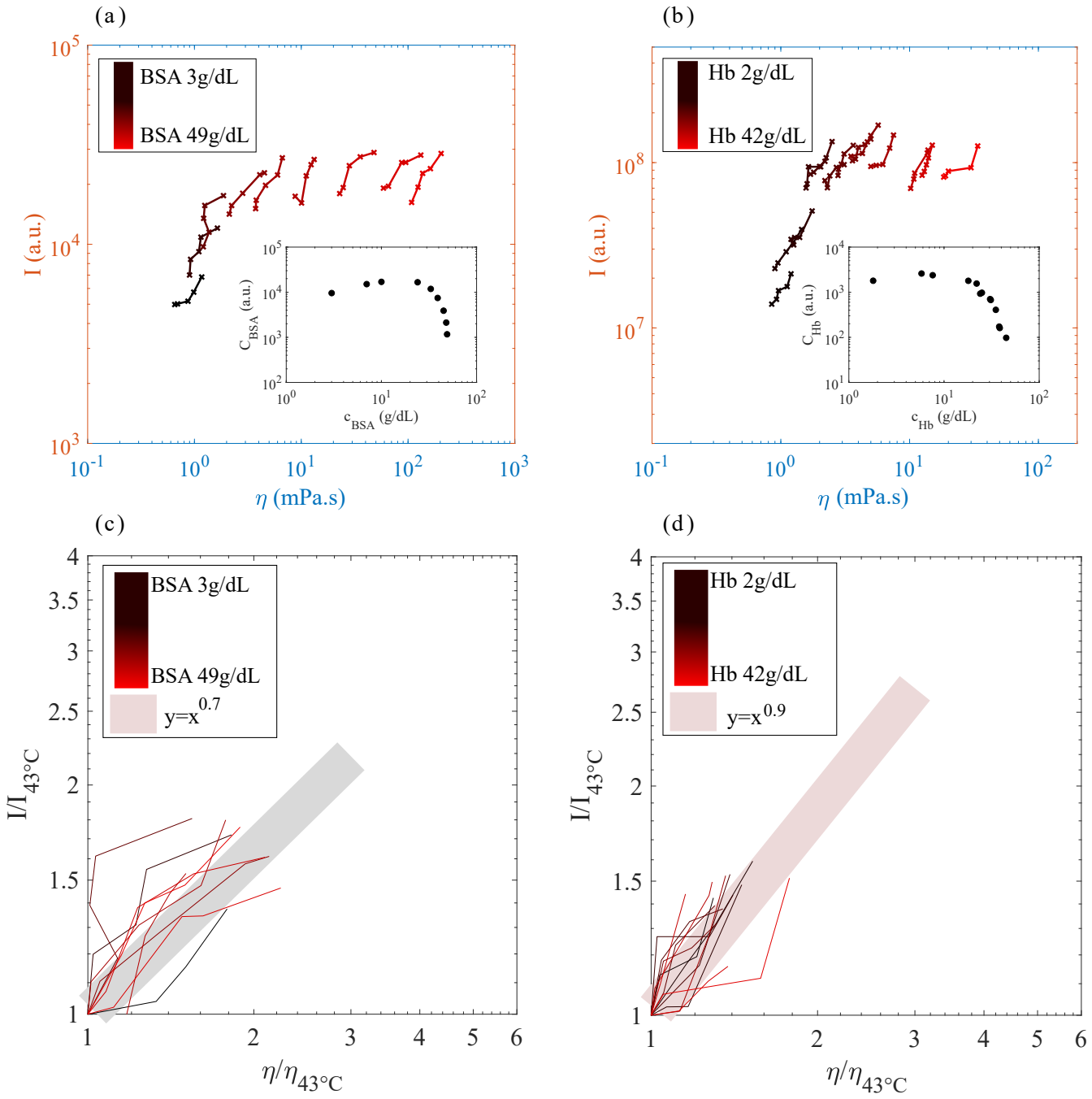

Figure 4. Intensity - viscosity curves by temperature variation in BSA (top left) and Hb (top right). The rotor fluorescence signal is measured at different protein concentrations. For each concentration, the temperature variation induces a viscosity variation. The data in Hb solutions are corrected for the absorbance term. The intensity-viscosity curves are plotted at the same origin and fitted with Förster-Hoffmann power laws of exponent 0.7 ± 0.2 in BSA (bottom left) and 0.9 ± 0.2 in Hb (bottom right). The margins of error are 5% for viscosity measurements and 7% for intensity measurements but are not shown here to simplify reading.

to the same parameter C in both cases. This result was also confirmed in previous studies where C could be assumed to be independent of temperature because the Förster-Hoffmann relationship reproduces the variations in intensity measured by temperature-induced viscosity variations[30]. In simple fluids, varying the temperature or concentration is therefore equivalent, and the viscosity was shown to be the predominant parameter that determines the rotor response[8,14].

In protein solutions however, we show that varying the viscosity with concentration or temperature is not equivalent for the

rotor. When the viscosity is varied with concentration in BSA and Hb, the fluorescence intensity of the rotor increases sharply at low concentration and reaches a plateau at high concentration. The intensity - viscosity curves follow a master curve combining the results obtained in the two protein solutions, and cannot be described by a Förster-Hoffmann power law. With concomitant microrheology mesurements, we show that the plateau is reached in the concentrated regime of the protein solution, beyond the semi-dilute regime, which is a first indication that the crowding of its environment has an influence on the rotor response. By varying the viscosity through temperature, we find Förster-Hoffmann power laws, $I = C\eta^x$, with the viscosity exponent $x = 0.7 - 0.9$ close to that measured in simple fluids. A major new feature in protein solutions is that the parameter C now depends on the concentration of the solution, unlike simple fluids, and decreases sharply beyond the semi-dilute protein regime. Because temperature and viscosity effects cannot be decoupled in this experiment, it cannot be excluded that the rotor response is influenced by temperature variation. Nevertheless, we have previously shown in PBS or in simple fluids[28] that when the viscosity is modified by temperature, the dominant parameter governing the DASPI signal is the viscosity of the medium. This suggests that temperature has little influence on the DASPI signal and validates our findings that concentration is the parameter to be considered in the rotor response.

In Figure 3, the Brownian bead response is used to define the boundary between the semi-dilute and concentrated regimes of the proteins. The boundary between the two regimes is quite visual. Typically, in the semi-dilute regime, an Einstein-Batchelor model can be applied to the viscosity and allows the protein size to be determined, and in the concentrated regime, the viscosity increases drastically with concentration. The rotor also shows different responses in the two regimes, with lower sensitivity in the concentrated regime. This highlights that the rotor response is determined by the crowding of the surrounding proteins.

Let us estimate the ratio rotor per protein to have an idea of the rotor environment in Figure 1. Given the experimental conditions, the number of molecules of BSA is 1.7 – respectively 17 and 170 – per molecule of DASPI at the crossover point (11 g/dL), when the rotor concentration is 1mM – respectively 0.1mM and 0.01mM. At the end of the plateau regime (49 g/dL), we have 7.6 molecules of BSA – respectively 76 and 760 – for 1 molecule of DASPI , when the rotor concentration is 1mM – respectively 0.1mM and 0.01mM. The very low concentration of the rotor relative to BSA suggests that the rotor response is dominated by surrounding protein crowding rather than specific rotor-protein interactions. This is consistent with the fact that it depends on the concentration regime of the protein solution, semi-dilute or concentrated.

A similar intensity-viscosity curve – increase then plateau – was measured with the CCVJ rotor in antibody solutions[3]. The dramatic increase in fluorescence intensity at low antibody concentration prior to the plateau was attributed to the binding of CCVJ to the antibody. In comparison, in our BSA solutions in Figure 1, the threshold between the increase regime and the plateau remains the same by varying the concentration of DASPI. This seems to exclude the hypothesis of a binding of the rotor to the BSA protein since one would expect a shift to a lower concentration as the rotor concentration increases.

In conclusion, in these protein solutions, the viscosity is not the parameter to be taken into account in the response of the rotor DASPI, the concentration appears to be a determining factor. At low rotor concentration compared to protein, which is the case in our experiments, the rotor signal is sensitive to the crowding of the protein solution and shows different responses in the semi-dilute and concentrated regimes. At a fixed concentration or given environment crowding, the rotor follows a Förster-Hoffmann power law with varying viscosity, $I = C\eta^x$ with C depending on the protein concentration in the solution. When the crowding varies, the intensity-viscosity curve deviates from the Förster-Hoffmann power law. This must be taken into account when using rotors in biofluids or complex fluids where the environment is complex at the rotor scale. Further research will probably shed light on the mechanisms of rotor-protein interaction in order to use these rotors quantitatively in biofluids.

A ANNEX : Molecular rotor in haemoglobin: correction of absorbance

The influence of Hb absorbance on the rotor fluorescence signal was corrected using a model based on the Beer-Lambert law, valid for Hb concentrations close to physiological concentrations[56]. We propose a theoretical expression for the intensity emitted by the rotor in a Hb solution placed in a standard measurement geometry of height L, under an inverted microscope (section A.1). This expression is validated experimentally using a triangular geometry of increasing height between 0 and L. This geometry allows us to probe the rotor response by increasing the height of the Hb solution and thus its degree of absorbance (section A.2). We propose with this model a corrective term for the absorbance of the Hb solution involving a screening length. The corrected intensity is proportional to the quantum yield of the DASPI molecules in the solution, and will be compared to the signal in non-absorbing proteins in section 3.1.1.

A.1 Measured intensity in the standard geometry

We consider here a Hb solution containing molecular rotors, observed under an inverted microscope in a standard measurement geometry represented in figure 5a, between a microscope slide and a coverslip separated by a spacer of height L. The molecular rotor is excited at a wavelength λ_{exc} and re-emits at a wavelength λ_{em}. The aim of this paragraph is to quantify the fluorescence intensity emitted by the molecular rotors and measured on the camera, I_{meas}, by considering the absorbance of the surrounding Hb solution.

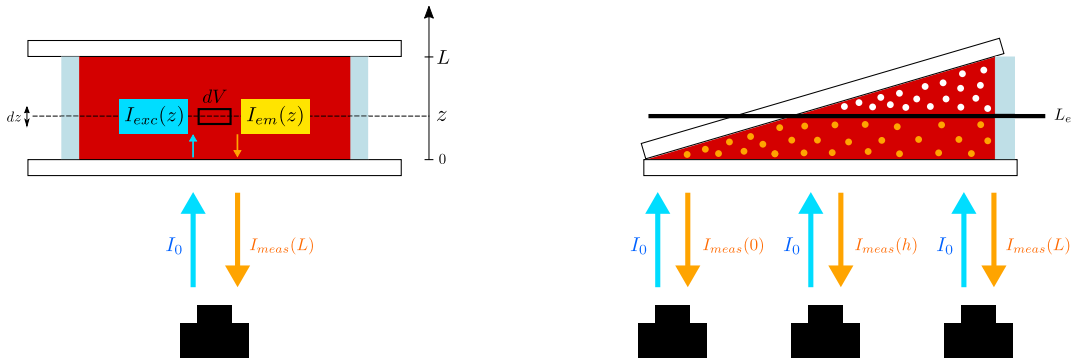

(a) (b)

Figure 5. (a) Standard geometry : the Hb solution is trapped between a microscope slide and a coverslip separated by a 250µm thick spacer. The incident beam intensity is I_0 and $I_{exc}(z)$, $I_{em}(z)$, $I_{meas}(L)$ are described in the text. (b) Triangle geometry : the Hb solution is trapped between two coverslips separated by a 250µm high spacer positioned on one side, creating a triangle geometry. Above a screening length L_e the molecules no longer receive an excitation signal due to the absorbance of the Hb below. The DASPI molecules in solution are represented by yellow and white dots. The yellow dots are those that receive an excitation signal, and the white ones are those that do not.

Let us consider a beam of excitation light of wavelength λ_{exc} and intensity I_0 coming initially from the microscope objective in the inverted configuration. We assume that this beam is cylindrical with a cross-section S. According to the Beer-Lambert law[57], a volume element $dV = S \cdot dz$ of the fluid at height z receives an excitation intensity $I_{exc}(z)$ lower than I_0 due to the absorbance of the solution over the height z :

$$I_{exc}(z) = I_0 \cdot 10^{-\varepsilon_{exc} \cdot z \cdot c_{Hb}}$$

with c_{Hb} the concentration of the Hb solution and $\varepsilon_{exc} = \varepsilon_{exc}(\lambda_{exc})$ the molar extinction coefficient of Hb at the exciting wavelength. This volume element contains $dN = \mathcal{N}_a \cdot c_{DASPI} \cdot dV$ DASPI molecules whose fluorescence emitting signal is proportional to the excitation intensity $I_{exc}(z)$ and to their quantum yield Φ. The intensity emitted by the molecular rotors in this volume element, at wavelength λ_{em}, is written :

$$I_{em}(z) = I_{exc}(z) \cdot \Phi \cdot dN$$

This emitted light still has once again to pass through a height z of hemoglobin, before being measured at the camera as I_{meas}, inducing a new Beer-Lambert correction term $10^{-\varepsilon_{em} \cdot z \cdot c_{Hb}}$ with $\varepsilon_{em} = \varepsilon_{em}(\lambda_{em})$ the molar extinction coefficient of Hb at the rotor emission wavelength. Since the camera collects the intensity coming from each volume element between $z = 0$ and $z = L$, we obtain for the measured intensity :

$$I_{mes}(L) = \int_0^L I_{em}(z) \cdot 10^{-\varepsilon_{em} \cdot z \cdot c_{Hb}} dz = \int_0^L I_0 \cdot \Phi \cdot \mathcal{N}_a \cdot c_{DASPI} \cdot S \cdot 10^{-(\varepsilon_{exc} + \varepsilon_{em}) \cdot z \cdot c_{Hb}} \cdot dz$$

which is also written :

$$I_{meas}(L) = P \cdot (1 - 10^{-L/L_e}) \tag{2}$$

with

$$L_e = \frac{1}{c_{Hb} \cdot (\varepsilon_{exc} + \varepsilon_{em})}; \quad P = \frac{I_0 \cdot \mathcal{N}_a \cdot c_{DASPI} \cdot S \cdot \Phi}{\ln(10)} \cdot L_e \tag{3}$$

L_e is interpreted as a screening length above which the DASPI molecules will receive no signal (white dots in Figure 5b) due to the high absorbance of the fluid below, and P as the plateau value that the fluorescence signal reaches for a fluid thickness L_e or more. In the limit where L_e tends to infinity ($L/L_e \to 0$), corresponding to the absence of screening by the absorbing molecules, the measured intensity in equation 2 is written to first order:

$$\lim_{L/L_e \to 0} I_{meas}(L) = P/L_e \cdot L \cdot \ln(10) = I_0 \mathcal{N}_a \cdot c_{DASPI} \cdot S \cdot L \cdot \Phi \tag{4}$$

which is proportional to the quantum yield Φ and corresponds to the intensity measured in a non-absorbing limit.

A.2 Model validation in triangular geometry

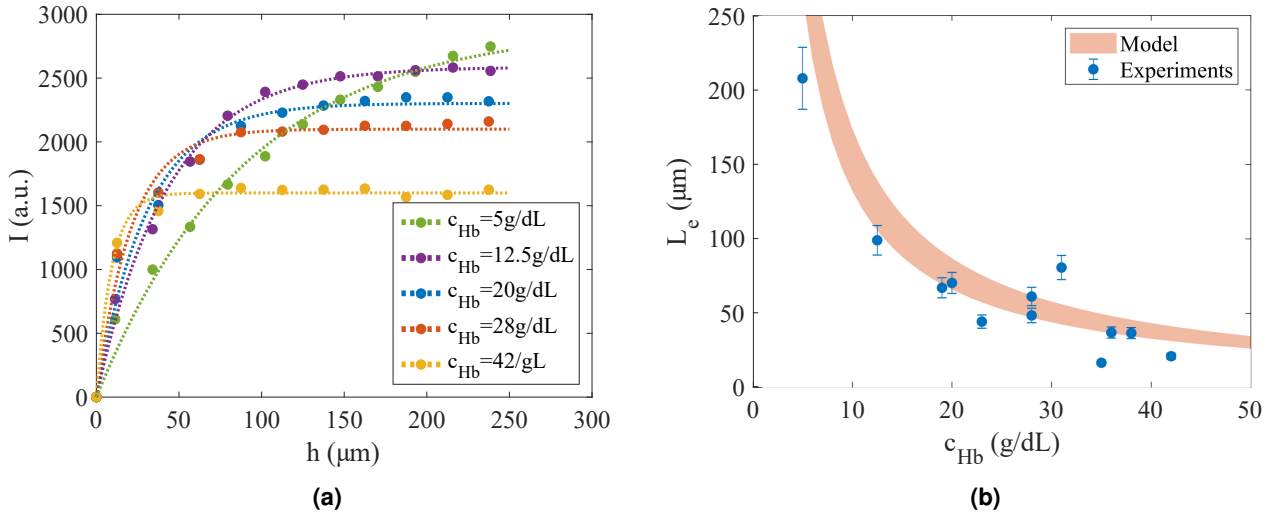

Figure 6. Model validation. (a) Fluorescence intensity $I_{meas}(h)$ of the DASPI rotor at concentration $c = 1$ mM, measured in the triangular geometry (coloured dots) for different Hb concentrations bewteen 5g/dL$\leq c_{Hb} \leq$ 42g/dL along with data fits with equation 2 (coloured dotted lines). (b) Screening length L_e obtained by fitting $I_{meas}(h)$ with the model equation 2 as a function of Hb concentration : theoretical and experimental values.

Our model was tested in a triangular geometry shown in figure 5b, consisting of a container of increasing thickness. In this geometry, Hb in trapped between two coverslips separated on one side by a $L = 250$µm high spacer. For a solution of Hb of given concentration, the intensity $I_{meas}(h)$ can be measured for layers of Hb of height h between $0 \leq h \leq L$, moving along the longitudinal axis of the container.

Figure 6a shows the fluorescence intensity evaluated for different heights h, in Hb solutions of concentration $c_{Hb} = 5, 12, 20, 28, 42$g/dL covering the range of interest. At all Hb concentrations, the fluorescence intensity could be fitted with excellent agreement using equation 2, with two parameters L_e and P. This experimentally demonstrates the existence of a screening length L_e above which a plateau value P for the fluorescence intensity emitted by the rotor is reached.

Figure 6b now shows the screening length L_e extracted from I_{meas} using equation 2, as a function of the Hb concentration c_{Hb}. The graph also shows the theoretical range for L_e using equation 3, by varying ε_{exc} between $2,67 \cdot 10^6 \text{m}^{-1}\cdot\text{M}^{-1}$ and $3,03 \cdot 10^6 \text{m}^{-1}\cdot\text{M}^{-1}$ and ε_{em} between $1,03 \cdot 10^6 \text{m}^{-1}\cdot\text{M}^{-1}$ and $1,85 \cdot 10^6 \text{m}^{-1}\cdot\text{M}^{-1}$. The ε-values were measured from absorbance spectra of diluted Hb (Varian Cary 50 UV-Vis spectrophotometer - Agilent) with uncertainties due to the width of the wavelength range selected by the fluorescence device: excitation $460-500$ nm, detection $565-625$ nm. The theoretical predicions (red band) for $L_e(c_{Hb})$ in Figure 6b show excellent agreement with the experimental data.

Our model (equations 2 and 3) is in excellent agreement with experimental data for I_{meas} and L_e, obtained in the triangular geometry. We propose to consider the quantity P/L_e as an intensity corrected for the influence of absorbance because it is directly proportional to the quantum yield Φ of the molecular rotors, as it is the case in non-absorbing limit (equation 4). We thus define the corrected fluorescence intensity as :

$$I_{corr}(L, c_{Hb}) = \frac{P}{L_e} = \frac{I_0 \cdot \mathcal{N}_a \cdot c_{DASPI} \cdot S}{\ln(10)} \cdot \Phi \tag{5}$$

By rewriting the above expression with equations 2 and 3, the expression for the corrected intensity is obtained from the measured intensity $I_{meas}(L)$, with a corrective term:

$$I_{corr}(L, c_{Hb}) = \frac{1}{L_e(c_{Hb}) \cdot \left(1 - 10^{-L/L_e(c_{Hb})}\right)} \cdot I_{meas}(L) \tag{6}$$

This correction involves two parameters to be known, the screening length L_e related to the Hb concentration c_{Hb} with equation 3, and the chamber height L. This correction will be used in the section 3.1.1 to compare the response of the rotor in absorbing and non-absorbing protein solution.

A.3 Data accessibility

Datasets for all experiments reported in this paper are available on FigShare (doi: 10.6084/m9.figshare.21512124[58]).

A.4 Author contribution

A.B. performed experiments. A. B. and B. A. consulted together on the interpretation of results and the preparation of the manuscript.

A.5 Declaration of Interests

The authors declare no competing interests.

A.6 Acknowledgements

The authors would like to thank Marc Durand and Olivia du Roure for the fruitful discussions.

References

1. Forster, T. & Hoffmann, G. Die viskositatsabhangigkeit der fluoreszenzquantenausbeuten einiger farbstoffsysteme. Zeitschrift fur Physikalische Chemie **75**, 63–76, DOI: 10.1524/zpch.1971.75.1_2.063 (1971).
2. Law, K. Fluorescence probe for microenvironments: anomalous viscosity dependence of the fluorescence quantum yield of p-n,n-dialkylaminobenzylidenemalononitrile in 1-alkanols. Chem. Phys. Lett. **75**, 545 – 549, DOI: https://doi.org/10.1016/0009-2614(80)80574-4 (1980).
3. Iwaki, T., Torigoe, C., Noji, M. & Nakanishi, M. Antibodies for fluorescent molecular rotors. Biochemistry **32**, 7589–7592, DOI: 10.1021/bi00080a034 (1993).
4. Loutfy, R. O. & Bradley, A. A. Effect of viscosity and temperature on torsional relaxation of molecular rotors. J. Phys. Chem. **86**, 4205–4211, DOI: https://doi.org/10.1021/j100218a023 (1982).
5. Kung, C. E. & Reed, J. K. Microviscosity measurements of phospholipid bilayers using fluorescent dyes that undergo torsional relaxation. Biochemistry **25**, 6114–6121, DOI: 10.1021/bi00368a042 (1986).
6. Haidekker, M. A., Brady, T., Lichlyter, D. & Theodorakis, E. Effects of solvent polarity and solvent viscosity on the fluorescent properties of molecular rotors and related probes. Bioorganic Chem. **33**, 415 – 425, DOI: https://doi.org/10.1016/j.bioorg.2005.07.005 (2005).
7. Wang, W., K.and Shi, Jia, J., Chen, S. & Ma, H. Characterization of 2-phenylbenzo[g]quinoxaline derivatives as viscosity-sensitive fluorescent probes. Talanta **77**, 1795 – 1799, DOI: https://doi.org/10.1016/j.talanta.2008.10.021 (2009).
8. Haidekker, M. A. & Theodorakis, E. A. Environment-sensitive behavior of fluorescent molecular rotors. J. biological engineering **4**, 1–14, DOI: 10.1186/1754-1611-4-11 (2010).
9. Haidekker, M. A. et al. Dyes with segmental mobility: molecular rotors. Adv. Fluoresc. Reporters Chem. Biol. I 267–308 (2010).
10. Loutfy, R. O. & Teegarden, D. M. Effect of polymer chain tacticity on the fluorescence of molecular rotors. Macromolecules **16**, 452–456, DOI: 10.1021/ma00237a022 (1983).
11. Zhu, D., Haidekker, M., Lee, J., Won, Y. & James, C. Application of molecular rotors to the determination of the molecular weight dependence of viscosity in polymer melts. Macromolecules **40**, 7730–7732, DOI: 10.1021/ma0702288 (2007).
12. Furuno, T. et al. A fluorescent molecular rotor probes the kinetic process of degranulation of mast cells. Immunol. Lett. **33**, 285 – 288, DOI: https://doi.org/10.1016/0165-2478(92)90074-X (1992).
13. Viriot, M. L. et al. Molecular rotors as fluorescent probes for biological studies. Clinical Hemorheology and Microcirculation **19**, 151–160 (1998).
14. Haidekker, M., L'Heureux, N. & Frangos, J. Fluid shear stress increases membrane fluidity in endothelial cells: a study with dcvj fluorescence. Am. J. Physiol. Circ. Physiol. **278**, H1401, DOI: 10.1152/ajpheart.2000.278.4.H1401 (2000).
15. Ma, C. et al. A minireview of viscosity-sensitive fluorescent probes: design and biological applications. J. Mater. Chem. B **8**, 9642–9651, DOI: 10.1039/D0TB01146K (2020).
16. Miao, W., Yu, C., Hao, E. & Jiao, L. Functionalized bodipys as fluorescent molecular rotors for viscosity detection. Front. chemistry **7**, 825, DOI: 10.3389/fchem.2019.00825 (2019).
17. Lee, S.-C. et al. Fluorescent molecular rotors for viscosity sensors. Chem. Eur. J. **24**, 13706–13718, DOI: 10.1002/chem.201801389 (2018).

18. Zhou, F. et al. Molecular rotors as fluorescent viscosity sensors: molecular design, polarity sensitivity, dipole moments changes, screening solvents, and deactivation channel of the excited states, DOI: 10.1002/ejoc.201100606 (2011).

19. Hawe, A., Filipe, V. & Jiskoot, W. Fluorescent molecular rotors as dyes to characterize polysorbate-containing igg formulations. Pharm. research **27**, 314–326, DOI: 10.1007/s11095-009-0020-2 (2010).

20. Kung, C. E. & Reed, J. K. Fluorescent molecular rotors: a new class of probes for tubulin structure and assembly. Biochemistry **28**, 6678–6686, DOI: 10.1021/bi00442a022 (1989). PMID: 2790023.

21. Sawada, S., Iio, T., Hayashi, Y. & Takahashi, S. Fluorescent rotors and their applications to the study of gf transformation of actin. Anal. biochemistry **204**, 110–117, DOI: 10.1016/0003-2697(92)90148-Z (1992).

22. Kubankova, M. et al. Probing supramolecular protein assembly using covalently attached fluorescent molecular rotors. Biomaterials **139**, 195–201, DOI: 10.1016/j.biomaterials.2017.06.009 (2017).

23. Thompson, A. J. et al. Molecular rotors provide insights into microscopic structural changes during protein aggregation. The J. Phys. Chem. B **119**, 10170–10179, DOI: 10.1021/acs.jpcb.5b05099 (2015).

24. Bai, Y. & Liu, Y. Illuminating protein phase separation: Reviewing aggregation-induced emission, fluorescent molecular rotor and solvatochromic fluorophore based probes. Chem. Eur. J. **27**, 14564–14576, DOI: 10.1002/chem.202102344 (2021).

25. Goh, W. L. et al. Molecular rotors as conditionally fluorescent labels for rapid detection of biomolecular interactions. J. Am. Chem. Soc. **136**, 6159–6162, DOI: 10.1021/ja413031h (2014).

26. Yu, W.-T., Wu, T.-W., Huang, C.-L., Chen, I.-C. & Tan, K.-T. Protein sensing in living cells by molecular rotor-based fluorescence-switchable chemical probes. Chem. science **7**, 301–307, DOI: 10.1039/C5SC02808F (2016).

27. Gatzogiannis, E. et al. Mapping protein-specific micro-environments in live cells by fluorescence lifetime imaging of a hybrid genetic-chemical molecular rotor tag. Chem. Commun. **48**, 8694–8696, DOI: 10.1039/C2CC33133K (2012).

28. Briole, A., Podgorski, T. & Abou, B. Molecular rotors as intracellular probes of red blood cell stiffness. Soft Matter **17**, 4525–4537, DOI: 10.1039/D1SM00321F (2021).

29. Liu, P., Zhu, Z., Zeng, C. & Nie, G. Specific absorption spectra of hemoglobin at different po_2 levels: potential noninvasive method to detect po_2 in tissues. J. Biomed. Opt. **17**, 125002, DOI: 10.1117/1.JBO.17.12.125002 (2012).

30. Howell, S., Dakanali, M., Theodorakis, E. A. & Haidekker, M. A. Intrinsic and extrinsic temperature-dependency of viscosity-sensitive fluorescent molecular rotors. J. fluorescence **22**, 457–465, DOI: 10.1007/s10895-011-0979-z (2012).

31. Haney, C. R., Buehler, P. W. & Gulati, A. Purification and chemical modifications of hemoglobin in developing hemoglobin based oxygen carriers. Adv. drug delivery reviews **40**, 153–169, DOI: 10.1016/S0169-409X(99)00047-2 (2000).

32. Waigh, T. A. Advances in the microrheology of complex fluids. Rep. Prog. Phys. **79**, 074601, DOI: 10.1088/0034-4885/79/7/074601 (2016).

33. Abou, B. et al. Extensive collection of femtolitre pad secretion droplets in the beetle leptinotarsa decemlineata allows nanolitre microrheology. J. R. Soc. Interface **7**, 1745–1752, DOI: 10.1098/rsif.2010.0075 (2010).

34. Colin, R. et al. Spatially heterogeneous dynamics in a thermosensitive soft suspension before and after the glass transition. Soft Matter **11**, 4504, DOI: 10.1039/c0sm01184c (2011).

35. Einstein, A. Über die von der molekularkinetischen theorie der wärme geforderte bewegung von in ruhenden flüssigkeiten suspendierten teilchen. Annalen der Physik **322**, 549–560 (1905).

36. Cheng, Z., Zhu, J., Chaikin, P. M., Phan, S. & Russel, W. B. Nature of the divergence in low shear viscosity of colloidal hard-sphere dispersions. Phys. Rev. E **64**, 041405, DOI: 10.1103/PhysRevE.65.041405 (2002).

37. Krieger, I. & Choi, G. Rheological studies on sterically stabilized model dispersions of uniform colloidal spheres : Ii. steady-shear viscosity. J. Colloid Interface Sci. **113**, 101–113, DOI: 10.1016/0021-9797(86)90210-9 (1986).

38. De Kruif, C. G., Van Lersel, E. M. F., Vrij, A. & Russel, W. B. Hard sphere colloidal dispersions : viscosity as a function of shear rate and volume fraction. The J. chemical physics **83**, 4717–4725, DOI: 10.1063/1.448997 (1985).

39. Parker, R., R., N. T., J., B. G., K., L. & G., R. S. The nonequilibrium phase and glass transition behavior of beta-lactoglobulin. Biophys. J. **89**, 1227 – 1236, DOI: 10.1529/biophysj.105.064246 (2005).

40. Brownsey, G. J., Noel, T. R., Parker, R. & Ring, S. G. The glass transition behavior of the globular protein bovine serum albumin. Biophys. journal **85**, 3943–3950, DOI: 10.1016/S0006-3495(03)74808-5 (2003).

41. Sharma, V., Jaishankar, A., Wang, Y.-C. & McKinley, G. H. Rheology of globular proteins: apparent yield stress, high shear rate viscosity and interfacial viscoelasticity of bovine serum albumin solutions. Soft Matter **7**, 5150, DOI: 10.1039/c0sm01312a (2011).

42. Foffi, G. et al. Hard sphere-like glass transition in eye lens α-crystallin solutions. Proc. Natl. Acad. Sci. **111**, 16748–16753, DOI: 10.1073/pnas.1406990111 (2014).

43. Garting, T. & Stradner, A. Optical microrheology of protein solutions using tailored nanoparticles. Small **14**, 1801548, DOI: 10.1002/smll.201801548 (2018).

44. Josephson, L. L., Furst, E. M. & Galush, W. J. Particle tracking microrheology of protein solutions. J. Rheol. **60**, 531–540, DOI: 10.1122/1.4948427 (2016).

45. Tu, R. S. & Breedveld, V. Microrheological detection of protein unfolding. Phys. Rev. E **72**, 041914, DOI: 10.1103/PhysRevE.72.041914 (2005).

46. Sarangapani, P. S., Hudson, S. D., Migler, K. B. & Pathak, J. A. The limitations of an exclusively colloidal view of protein solution hydrodynamics and rheology. Biophys. journal **105**, 2418–2426, DOI: 10.1016/j.bpj.2013.10.012 (2013).

47. Stradner, A. & Schurtenberge, P. Potential and limits of a colloid approach to protein solutions. Soft Matter **16**, 307–323, DOI: 10.1039/c9sm01953g (2020).

48. Batchelor, G. K. The effect of brownian motion on the bulk stress in a suspension of spherical particles. J. Fluid Mech. **83**, 97–117, DOI: 10.1017/S0022112077001062 (1977).

49. Mooney, M. The viscosity of a concentrated suspensions of spherical particles. J. Colloid Sci. **6**, 162–170, DOI: 10.1016/0095-8522(51)90036-0 (1951).

50. Krieger, M. & Dougherty, T. J. A mechanism for non-newtonian flow in suspensions of rigid spheres. J. Rheol. **3**, 137–152, DOI: 10.1122/1.548848 (1959).

51. Jachimska, B., Wasilewska, M. & Adamczyk, Z. Characterization of globular protein solutions by dynamic light scattering, electrophoretic mobility, and viscosity measurements. Langmuir **24**, 6866 – 6872, DOI: 10.1021/la800548p (2008).

52. Stadler, A. M. et al. Hemoglobin dynamics in red blood cells: correlation to body temperature. Biophys. journal **95**, 5449–5461, DOI: 10.1529/biophysj.108.138040 (2008).

53. Digel, I. et al. Body temperature-related structural transitions of monotremal and human hemoglobin. Biophys. journal **91**, 3014–3021, DOI: 10.1529/biophysj.106.087809 (2006).

54. Arosio, D., Kwansa, H. E., Gering, H., Piszczek, G. & Bucci, E. Static and dynamic light scattering approach to the hydration of hemoglobin and its supertetramers in the presence of osmolites. Biopolym. Orig. Res. on Biomol. **63**, 1–11, DOI: 10.1002/bip.1057 (2002).

55. Haidekker, M. A. & Theodorakis, E. A. Molecular rotors—fluorescent biosensors for viscosity and flow. Org. & Biomol. Chem. **5**, 1669–1678, DOI: 10.1039/B618415D (2007).

56. Friebel, M. & Meinke, M. C. Determination of the complex refractive index of highly concentrated hemoglobin solutions using transmittance and reflectance measurements. J. Biomed. Opt. **10**, 064019, DOI: 10.1117/1.2138027 (2005).

57. Valeur, B. & Berberan-Santos, M. N. Molecular Fluorescence: Principles and Applications (Wiley, 2012), 1 edn.

58. Briole, A. & Abou, B. Data file from the experiments presented in the article 'molecular rotors in hb and BSA proteins', DOI: 10.6084/M9.FIGSHARE.21512124. Artwork Size: 28179 Bytes Pages: 28179 Bytes Type: dataset.